Knotting statistics for polygons in lattice tubes

N. R. Beaton
School of Mathematics and Statistics
The University of Melbourne, Victoria 3010, Australia

J. W. Eng C. E. Soteros*
Department of Mathematics and Statistics
The University of Saskatchewan, Saskatoon, SK, Canada S7N 5E6

March 29, 2019

Abstract

We study several related models of self-avoiding polygons in a tubular subgraph of the simple cubic lattice, with a particular interest in the asymptotics of the knotting statistics. Polygons in a tube can be characterised by a finite transfer matrix, and this allows for the derivation of pattern theorems, calculation of growth rates and exact enumeration. We also develop a static Monte Carlo method which allows us to sample polygons of a given size directly from a chosen Boltzmann distribution.

Using these methods we accurately estimate the growth rates of unknotted polygons in the $2 \times 1 \times \infty$ and $3 \times 1 \times \infty$ tubes, and confirm that these are the same for any fixed knot-type K. We also confirm that the entropic exponent for unknots is the same as that of all polygons, and that the exponent for fixed knot-type K depends only on the number of prime factors in the knot decomposition of K. For the simplest knot-types, this leads to a good approximation for the polygon size at which the probability of the given knot-type is maximized, and in some cases we are able to sample sufficiently long polygons to observe this numerically.

Dedicated to Stuart Whittington on the occasion of his 75$^{\text{th}}$ birthday.

1 Introduction

Self-avoiding walk and self-avoiding polygon models are the standard statistical mechanics lattice models for linear and ring polymers in dilute solutions [1, 2]. They are also of interest due to their connection with critical phenomena for other lattice models of statistical mechanics [3, 4]. Initial studies of self-avoiding polygon models focused on studying polygon counts and average geometric properties (e.g. radius of gyration) via exact enumeration, theoretical analysis and Monte Carlo sampling. For example, early contributions of S. G. Whittington to the field contributed in all three of these aspects [5, 6]. Subsequently, interest in studying the average topological properties of polygons has grown. This interest arose from the seminal paper by Sumners and Whittington [7], where they used a lattice polygon model to establish the long-standing Frisch-Wasserman-Delbruck (FWD) [8, 9] conjecture that sufficiently long ring polymers have a high probability of being knotted. Continued interest related to this has been motivated by a concomitant growth in experimental data related to DNA topology (see for example the review articles [10, 11] and references therein).

*soteros@math.usask.ca

Early numerical studies of knotting probabilities for lattice polygons were due to Janse van Rensburg and Whittington [12] using Markov chain Monte Carlo simulations of fixed-length polygons on the fcc lattice. Some corresponding off-lattice results were subsequently obtained by Katrich et al. [13] as well as Shimamura and Deguchi [14]. From such off-lattice studies [14, 15, 16], Deguchi and co-workers proposed a general asymptotic form for the probability of a given knot-type K as a function of polygon length n:

$$\mathbb{P}_n(K) \sim A_K(n - \Delta N(K))^{m(K)} \exp\left(-\frac{n - \Delta N(K)}{N_K}\right), \qquad n \to \infty, \tag{1}$$

where $A_K, \Delta N(K), m(K)$ and N_K are expected to be constants which may depend on K but not n. This form is consistent with lattice evidence [17, 18, 19, 20, 21, 22] that indicates that $p_n(K)$, the number of n-edge self-avoiding polygons (counted up to translation) with fixed knot-type K, has the following asymptotic form:

$$p_n(K) \sim C_K \mu_{0_1}^n n^{\alpha_{0_1} - 3 + f_K}, \qquad \text{as} \quad n \to \infty, \tag{2}$$

where $f_{0_1} = 0$ and otherwise f_K is the number of prime knot factors (*factors*, for short) in the prime knot decomposition of knot-type K and where μ_{0_1} is the lattice-dependent *growth constant* for unknotted polygons (μ_{0_1} is proved to exist in [7]). For all polygons, the conjectured asymptotics are

$$p_n = \sum_K p_n(K) \sim C\mu^n n^{\alpha - 3}, \qquad \text{as} \quad n \to \infty, \tag{3}$$

with the growth constant $\mu > \mu_{0_1}$ (this strict inequality is established in the proof of the FWD conjecture [7]). For lattice polygons, there is evidence that the unknot entropic exponent $\alpha_{0_1} = \alpha$; hence in the case that each n-edge lattice polygon is considered to be equally likely, (2) and (3) lead to a conjectured asymptotic form consistent with (1):

$$\begin{aligned} \mathbb{P}_n(K) &= \frac{p_n(K)}{p_n} \\ &\sim A_K(n - \Delta N(K))^{f_K} \exp[-(n - \Delta N(K))(\log \mu - \log \mu_{0_1})], \end{aligned} \tag{4}$$

with $m(K) = f_K$ and $N_K = N_{0_1} = (\log \mu - \log \mu_{0_1})^{-1}$. There is also numerical evidence from lattice models that the amplitude ratios $C_{K_1}/C_{K_2} = A_{K_1}/A_{K_2}$ for different prime knots K_1 and K_2 are lattice-independent (i.e. universal) [20]. However, recent evidence for an off-lattice model (which allows for varying a cylindrical radius of excluded volume) indicates that these amplititude ratios may depend on the extent (the radius) of excluded-volume in the model [16]. Without excluded volume, numerical results [23] for equilateral off-lattice polygons support the following form for $\mathbb{P}_n(0_1)$,

$$\mathbb{P}_n(0_1) \sim A_{0_1} n^{m(0_1)} e^{-n/N_{0_1}} \left(1 + \frac{B}{n^\Delta} + \frac{C}{n}\right), \qquad n \to \infty, \tag{5}$$

with estimates for $\Delta \approx 1/2$ and $m(0_1) \approx -0.125$, indicating that $m(0_1) < 0$ for this model while for lattice polygons $m(0_1)$ is expected to be 0.

Using the form of equation (4), for any fixed K, $\mathbb{P}_n(K)$ decays exponentially to zero as $n \to \infty$ but for any $K \neq 0_1$, $\mathbb{P}_n(K)$ will increase initially with n, reaching a maximum at $n \approx \Delta N(K) + f_K N_{0_1}$ before decaying. Consistent with this, numerical evidence from various lattice and off-lattice models indicates that for a given model and for the simplest knots, $N_{0_1} \gg \Delta N(K)$ and the knot-type dependence of the location of the maximum depends primarily on f_K, the number of prime knot factors in the prime-knot decomposition of K. Note however

that $\Delta N(K)$ is expected to depend on the minimum number of edges needed to create the knot, and hence it is generally non-zero, dependent on K and does contribute to the location of the maximum.

Parallel to the interest in polymer entanglement complexity, there has also been interest in the properties of lattice models of polymers in confined geometries (see for example reviews in [24, 25, 1, 11]). The nature of the confinement considered has ranged from partial confinement in wedges, slabs or tubes (prisms), where the polymer is allowed to extend freely in one or more direction, to full confinement in a sphere or box. Initial studies [26, 27, 28, 29] focused on the effects of confinement on limiting free energies, entropic exponents and geometric properties. Recent interest has turned to studying the effects on knotting statistics. Respective versions of the FWD conjecture have been proved for wedges [30], slabs [31, 32] and tubes [33], and knotting statistics are believed to follow asymptotic forms similar to those given above. Other studies have considered the effect of confinement on the "size" of the knotted part and the extent of localization of the knot [34].

In general, for most lattice polygon models, little can be proved about the asymptotic forms (2), (3), (4) beyond the existence of growth constants for all and unknotted polygons and the corresponding FWD conjecture proof. However, in the case of polygons confined to any $L \times M \times \infty$ simple-cubic lattice tube, it is known [33] via transfer matrix arguments that

$$p_{\mathbb{T},n} \sim C_{\mathbb{T}} \mu_{\mathbb{T}}^n, \qquad \text{as} \quad n \to \infty, \tag{6}$$

where $p_{\mathbb{T},n}$ counts the number of n-edge polygons in a given tube $\mathbb{T}$ (up to translation in the direction of the infinite axis of the tube) and the constants $C_{\mathbb{T}}$ and $\mu_{\mathbb{T}}$ are determined by the eigenvectors and eigenvalues of the transfer matrix. Very recently, for the smallest such tube that admits non-trivial knots ($2 \times 1 \times \infty$), for knots K in the set of all 2-bridge knots with unknotting number one or knots formed from their connect-sum, it has been established [35] for n sufficiently large that there exist constants B_K, b_K, D_K and d_K such that

$$B_K p_{\mathbb{T},n-b_K}(0_1) n^{f_K} \leq p_{\mathbb{T},n}(K) \leq D_K p_{\mathbb{T},n+d_K}(0_1) n^{f_K}, \tag{7}$$

where $p_{\mathbb{T},n}(K)$ is the number of polygons counted in $p_{\mathbb{T},n}$ that have knot-type K. This establishes the expected form from (2) for the growth constant and the increase in the entropic exponent. The arguments used for this, however, do not appear to be easily extended to other knot-types or larger tube sizes. Consistent with (2) and (7), it is conjectured that for any knot K,

$$p_{\mathbb{T},n}(K) \sim C_{\mathbb{T},K} n^{f_K} \mu_{\mathbb{T},0_1}^n, \qquad \text{as} \quad n \to \infty. \tag{8}$$

In this paper, we explore some of the remaining open questions about the knotting statistics in tubes by using transfer matrix arguments, exact enumeration and Monte Carlo methods for tube sizes $L \times 1 \times \infty$ for $L = 2$ and 3. In particular, we provide numerical evidence that (8) holds and that the entropic exponent for unknots is the same as that for all polygons, i.e. that there exist constants $C_{\mathbb{T},0_1}$ and $\mu_{\mathbb{T},0_1}$ consistent with

$$p_{\mathbb{T},n}(0_1) \sim C_{\mathbb{T},0_1} \mu_{\mathbb{T},0_1}^n, \qquad \text{as} \quad n \to \infty. \tag{9}$$

Our evidence is primarily based on counts of polygons in tubes enumerated by maximum span s (in the unconfined direction) instead of by number of edges n; the asymptotic forms of (8) and (9) should not depend on whether s or n is used but the constants in these equations are expected to change.

The scaling form of (2) is consistent with the idea that, on average, sufficiently long ring polymers with a fixed knot-type K have entropy similar to that of "decorated" unknots for which

a typical configuration has the prime factors of the knot being relatively localized and randomly distributed throughout an otherwise unknotted polymer ring (ie roughly there are $\binom{n}{f_K} \approx n^{f_K}$ places to put the factors along the length n polymer) [21]. Our results in this paper regarding (8) and (9) indicate that this idea still holds even under fairly tight tubular confinement (such as well-below the de Gennes scaling regime [34]) and even for highly compressed or dense polymers (modelled here by Hamiltonian polygons). This is also consistent with our observations in [34] where, although we classify different types of knot patterns as "local" versus "non-local" and observe that "non-local" patterns are more likely, we also observe that the average sizes of knot patterns when they occur (regardless of their type) are relatively small compared to the length of the polygon.

The outline of the paper is as follows. In Section 2 we define a general model of self-avoiding polygons confined to a lattice tube, with Boltzmann weights associated with length and/or span along the axis of the tube. In Section 3 we describe how transfer matrices can be used to study this model, and introduce a Monte Carlo algorithm for sampling random polygons directly from the desired Boltzmann distribution. Section 4 contains a variety of numerical results, including enumerations and growth rates obtained directly from the transfer matrices, and estimates of knotting probabilities, unknot growth rates, critical exponents and amplitude ratios obtained via simulation. These results are used to provide evidence for the asymptotic forms (8) and (9). Finally some concluding remarks are given in Section 5.

2 Theory and exact results

To begin we need some definitions. For non-negative integers L, M, let $\mathbb{T}_{L,M} \equiv \mathbb{T} \subset \mathbb{Z}^3$ be the semi-infinite $L \times M$ tube on the simple cubic lattice defined by

$$\mathbb{T} = \{(x, y, z) \in \mathbb{Z}^3 : x \geq 0, 0 \leq y \leq L, 0 \leq z \leq M\}.$$

2.1 The fixed-edge model

We consider first a general model for polymers in tubes where the polymer (modelled by a polygon in a lattice tube) is subject to an external force. This model has been studied previously – see [36] and references therein. The notation and definitions used here (unless stated otherwise) are as in [36]. Define $\mathcal{P}_{\mathbb{T}}$ to be the set of self-avoiding polygons in $\mathbb{T}$ which occupy at least one vertex in the plane $x = 0$, and let $\mathcal{P}_{\mathbb{T},n}$ be the subset of $\mathcal{P}_{\mathbb{T}}$ comprising polygons with n edges (n even). Then let $p_{\mathbb{T},n} = |\mathcal{P}_{\mathbb{T},n}|$.

We define the *span* $s(\pi)$ of a polygon $\pi \in \mathcal{P}_{\mathbb{T}}$ to be the maximal x-coordinate reached by any of its vertices and we use $|\pi|$ to denote the number of edges in π. See Figure 1 for a polygon π that fits in a 2×1 tube with $s(\pi) = 6$ and $|\pi| = 36$. Let $p_{\mathbb{T},n}(s)$ be the number of polygons in $\mathcal{P}_{\mathbb{T},n}$ with span s. To model a force acting parallel to the x-axis, we introduce a fugacity conjugate to polygon span which yields a Boltzmann weight, $e^{fs(\pi)}$, for each polygon π. Then the "fixed-edge" model partition function is given by

$$Z_{\mathbb{T},n}(f) = \sum_{|\pi|=n} e^{fs(\pi)} = \sum_{s} p_{\mathbb{T},n}(s) e^{fs}. \tag{10}$$

For this model, the probability of a polygon $\pi \in \mathcal{P}_{\mathbb{T},n}$ is given by

$$\mathbb{P}_n^{(\mathrm{ed},f)}(\pi) = \frac{e^{fs(\pi)}}{Z_{\mathbb{T},n}(f)}. \tag{11}$$

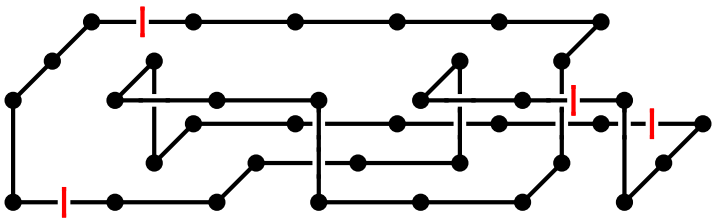

Figure 1: A 36-edge polygon π that fits inside $\mathbb{T}_{L,M}$ with $L \geq 2$ and $M \geq 1$; the tube extends without bound to the right and the span $s(\pi) = 6$. The locations of the two pairs of vertical red lines divide the polygon into connect-sum patterns; in this example, the polygon can be decomposed into a start unknot pattern on the left, a proper connect-sum trefoil knot pattern in the middle, and an end unknot pattern on the right.

Thus $f \ll 0$ corresponds to the "compressed" regime while $f \gg 0$ corresponds to the "stretched" regime.

The (limiting) *free energy per edge* of polygons in $\mathbb{T}$ is defined as

$$\mathcal{F}_{\mathbb{T}}(f) = \lim_{n\to\infty} \frac{1}{n} \log Z_{\mathbb{T},n}(f).$$

This is known [37] to exist for all f.

For $f = 0$, it has been proved that [38, 28]

$$\begin{aligned} \mathcal{F}_{\mathbb{T}}(0) = \log \mu_{\mathbb{T}} &= \lim_{n\to\infty} n^{-1} \log p_{\mathbb{T},n} \\ &< \lim_{n\to\infty} n^{-1} \log c_{\mathbb{T},n} \\ &< \lim_{n\to\infty} n^{-1} \log p_n = \lim_{n\to\infty} n^{-1} \log c_n \equiv \log \mu, \end{aligned} \tag{12}$$

where c_n is the number of n-step self-avoiding walks (SAWs) in $\mathbb{Z}^3$ starting at the origin and μ is their growth constant, and $c_{\mathbb{T},n}$ is the number of these confined to $\mathbb{T}$.

A subset of self-avoiding polygons in $\mathbb{T}$ are *Hamiltonian* polygons: those which occupy every vertex in a $s \times L \times M$ subtube of $\mathbb{T}$. In addition to being a useful lower bound for general polygons in the $f < 0$ compressed regime, these also serve as an idealized model of tightly packed ring polymers [39]. We define the number of Hamiltonian polygons, $p^{\mathrm{H}}_{\mathbb{T},n}$, to be the number of n-edge polygons in $\mathcal{P}_{\mathbb{T},n}$ which have span s and occupy every vertex in an $s \times L \times M$ subtube of $\mathbb{T}$. Defining $W_{\mathbb{T}} = (L+1)(M+1)$ (the number of vertices in an integer plane $x = i \geq 0$ of the tube), we assume without loss of generality that $L \geq M$; note that $p^{\mathrm{H}}_{\mathbb{T},n} = 0$ if n (even) is not a multiple of $W_{\mathbb{T}}$. The following limit has been proved to exist [36] (see also [40]):

$$\kappa^{\mathrm{H}}_{\mathbb{T}} = \log \mu^{\mathrm{H}}_{\mathbb{T}} \equiv \lim_{s\to\infty} \frac{1}{(s+1)W_{\mathbb{T}}} \log p^{\mathrm{H}}_{\mathbb{T},(s+1)W_{\mathbb{T}}}. \tag{13}$$

Furthermore, using this, $\mathcal{F}_{\mathbb{T}}(f)$, the free energy per edge, is bounded as follows:

$$\max\{f/2, (f/W_{\mathbb{T}}) + \kappa^{\mathrm{H}}_{\mathbb{T}}\} \leq \mathcal{F}_{\mathbb{T}}(f) \leq \max\{f/W_{\mathbb{T}}, f/2\} + \mathcal{F}_{\mathbb{T}}(0), \tag{14}$$

with $\mathcal{F}_{\mathbb{T}}(f)$ asymptotic to the lower bound for $f \to \infty$ for any $\mathbb{T}$, and for $f \to -\infty$ for small tube sizes (this is conjectured to be true for any $\mathbb{T}$), see [36]. More specifically, in [36] it is established that:

$$\lim_{f\to-\infty} \mathcal{F}_{\mathbb{T}}(f) = \beta^{\mathrm{F}}_{\mathbb{T}}/W_{\mathbb{T}}, \tag{15}$$

where β^{F} is the exponential growth rate (as span $s \to \infty$) for full s-patterns (defined later in Section 3.1 and (36)). It was also established that $\beta^{\mathrm{F}}_{\mathbb{T}}/W_{\mathbb{T}} = \kappa^{\mathrm{H}}_{\mathbb{T}}$ for all tubes such that $5 \geq L \geq M \geq 0$.

2.2 The fixed-span model

Here, we will also be interested in the dual model, called the "fixed-span" model, with partition function given by

$$Q_{\mathbb{T},s}(g) = \sum_n p_{\mathbb{T},n}(s) e^{gn},$$

and where the probability associated with a span s polygon π is given by

$$\mathbb{P}_s^{(\mathrm{sp},g)}(\pi) = \frac{e^{g|\pi|}}{Q_{\mathbb{T},s}(g)}. \tag{16}$$

For this model, when $g \gg 0$ densely packed (in terms of number of edges per span) polygons dominate the partition function, while when $g \ll 0$ polygons with very few edges per span dominate. The associated (limiting) *free energy per span* exists [36] (see also [41]):

$$\mathcal{G}_{\mathbb{T}}(g) = \lim_{s\to\infty} \frac{1}{s} \log Q_{\mathbb{T},s}(g). \tag{17}$$

For brevity we will introduce quantities analogous to $\kappa_{\mathbb{T}}$ and $\mu_{\mathbb{T}}$:

$$\chi_{\mathbb{T}} = \log \nu_{\mathbb{T}} = \mathcal{G}_{\mathbb{T}}(0). \tag{18}$$

Note also that Hamiltonian polygons can be counted by span. But for these the length is a constant multiple of the span, so we have the simple relation

$$\chi_{\mathbb{T}}^{\mathrm{H}} = \log \nu_{\mathbb{T}}^{\mathrm{H}} = \lim_{s\to\infty} \frac{1}{s} \log p_{\mathbb{T},(s+1)W_{\mathbb{T}}}^{\mathrm{H}} = W_{\mathbb{T}} \kappa_{\mathbb{T}}^{\mathrm{H}}. \tag{19}$$

Both the fixed-edge and fixed-span models correspond to special cases of the grand canonical partition function

$$G_{\mathbb{T}}(f,g) = \sum_s \sum_n p_{\mathbb{T},n}(s) e^{gn+fs}$$

and can be studied using transfer matrix methods [41].

Hamiltonian polygons can also be studied using transfer matrices [36, 40] and we will also investigate the fixed-span model where polygons are restricted to being Hamiltonian. In that case, the probability associated with a span s Hamiltonian polygon π is given by

$$\mathbb{P}_s^{\mathrm{H}}(\pi) = \frac{1}{p_{\mathbb{T},(s+1)W_{\mathbb{T}}}^{\mathrm{H}}}. \tag{20}$$

2.3 Knotting statistics in tubes - theory and exact results

In terms of knotting statistics for these models, the FWD conjecture has been proved. For this, there are known "pattern theorems" available for the fixed-edge and fixed-span models (see [41, 37]), as well as for Hamiltonian polygons (see [40]). The theorems focus on proper polygon patterns (see [36] for more precise definitions). Given a proper pattern P which can occur in a polygon in $\mathbb{T}$, define $p_{\mathbb{T},n}(s;P,m)$ to be the number of polygons counted in $p_{\mathbb{T},n}(s)$ which contain at most m translates of P. Then we have that, for any fixed f and proper polygon pattern P, there exists $\epsilon_P > 0$ such that:

$$\begin{aligned}\mathcal{F}_{\mathbb{T}}(f;P,\epsilon_P) &\equiv \limsup_{n\to\infty} \frac{1}{n} \log Z_{\mathbb{T},n}(f;P,\epsilon_P) \\ &\equiv \limsup_{n\to\infty} \frac{1}{n} \log \sum_s p_{\mathbb{T},n}(s;P,\epsilon_P n) e^{fs} < \mathcal{F}_{\mathbb{T}}(f).\end{aligned} \tag{21}$$

So for n sufficiently large, all but exponentially few n-edge polygons subjected to the force f contain more than $\epsilon_P n$ copies of P. Similarly for any fixed g and proper polygon pattern P, there exists $\tilde{\epsilon}_P > 0$ such that:

$$\begin{aligned}\mathcal{G}_{\mathbb{T}}(g; P, \tilde{\epsilon}_P) &\equiv \limsup_{s\to\infty} \frac{1}{s} \log Q_{\mathbb{T},s}(g; P, \tilde{\epsilon}_P) \\ &\equiv \limsup_{s\to\infty} \frac{1}{s} \log \sum_n p_{\mathbb{T},n}(s; P, \tilde{\epsilon}_P s) e^{gn} < \mathcal{G}_{\mathbb{T}}(g). \end{aligned} \tag{22}$$

Finally, for any proper Hamiltonian polygon pattern P (see [40]), there exists $\hat{\epsilon}_P > 0$ such that:

$$\limsup_{n\to\infty} p^{\mathrm{H}}_{\mathbb{T},n}(P, \hat{\epsilon}_P n) < \kappa^{\mathrm{H}}_{\mathbb{T}}. \tag{23}$$

So all but exponentially few sufficiently long n-edge Hamiltonian polygons contain more than $\hat{\epsilon}_P n$ copies of P.

In a previous study [34] we defined *connect-sum* knot patterns for polygons in tubes. This concept will be useful in the present article, so we briefly review the definition here. For $k \in \mathbb{N}$, we say a polygon π in $\mathbb{T}$ has a *2-section* at $k+\frac{1}{2}$ if π intersects the plane $x = k+\frac{1}{2}$ at exactly two points. If π has t 2-sections, then it can be partitioned into $t+1$ pieces – these are *connect-sum patterns* (so named because they give an easy way of writing the polygon as the connect-sum of smaller pieces). If $t \geq 1$ then the first and last are *start* and *end* connect-sum patterns; the remainder (if any) are *proper* connect-sum patterns. (Figure 1 shows a polygon divided into a start, proper and end connect-sum pattern.) Any connect-sum pattern can be converted into a closed curve by joining any pairs of loose ends at the left and at the right; note that if the resulting closed curve has knot-type K then K must be part of the knot decomposition of the original polygon.

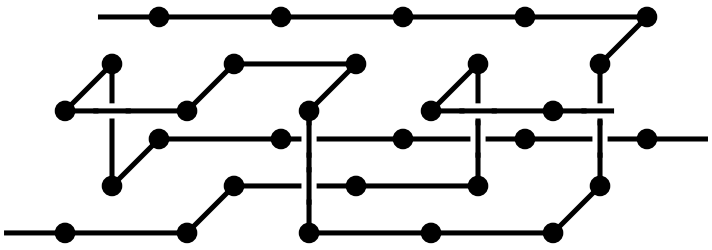

Figure 2: A minimal-size Hamiltonian connect-sum trefoil pattern in the 2×1 tube. This is one of the 32 counted in the first row of Table 1.

Figure 2 shows an example of a smallest connect-sum trefoil knot pattern that can occur in a Hamiltonian polygon in a 2×1 tube. Similar knot patterns can be found for any tube size, so that the pattern theorems of (21)-(23) can be used to establish that all but exponentially few sufficiently long polygons (regardless of the model and the fixed value of f or g), are knotted. From such theorems it can also be shown (using arguments analogous to those in [42]) that the knot-complexity of polygons grows as polygon "size" grows (size could be measured in terms of edges or span), so that a typical polygon will have a highly-composite knot-type $K = K_1 \# K_2 \# \ldots \# K_r$. Furthermore, for each model, if polygons are restricted to being unknots, the resulting limiting free energy exists and is strictly less than the corresponding limiting free energy for all polygons in the model. In particular, respectively for the $f = 0$ fixed-edge, $g = 0$ fixed-span, and the Hamiltonian models, it is known that (see [41, 37, 40]) the following limits exist and satisfy:

$$\kappa_{\mathbb{T},0_1} = \log \mu_{\mathbb{T},0_1} \equiv \lim_{n\to\infty} \frac{1}{n} \log p_{\mathbb{T},n}(0_1) < \kappa_{\mathbb{T}}; \tag{24}$$

Table 1: Numbers (counts) of trefoil patterns of smallest spans in the 2×1 and 3×1 tubes; counts are given by span for all patterns, Hamiltonian patterns and full patterns.

Tube Size	Span	Count	Ham. Count	Full Count
2×1	5	116	32	36
	6	5,888	748	788
	7	156,224	9,408	9,928
3×1	3	1,964	232	276
	4	792,256	19,016	22,888

$$\chi_{\mathbb{T},0_1} = \log \nu_{\mathbb{T},0_1} \equiv \lim_{s\to\infty} \frac{1}{s} \log q_{\mathbb{T},s}(0_1) < \chi_{\mathbb{T}}, \tag{25}$$

where $q_{\mathbb{T},s}(K)$ is the number of knot-type K span-s polygons in $\mathbb{T}$ counted up to x-translation; and

$$\kappa^{\mathrm{H}}_{\mathbb{T},0_1} = \log \mu^{\mathrm{H}}_{\mathbb{T},0_1} \equiv \lim_{s\to\infty} \frac{1}{(s+1)W_{\mathbb{T}}} \log p^{\mathrm{H}}_{\mathbb{T},(s+1)W_{\mathbb{T}}}(0_1) < \kappa^{\mathrm{H}}_{\mathbb{T}}, \tag{26}$$

where $p^{\mathrm{H}}_{\mathbb{T},n}(K)$ is the number of n-edge knot-type K Hamiltonian polygons in $\mathbb{T}$ counted up to x-translation. We also have $\chi^{\mathrm{H}}_{\mathbb{T},0_1} \equiv \log \nu^{\mathrm{H}}_{\mathbb{T},0_1} \equiv W_{\mathbb{T}} \kappa^{\mathrm{H}}_{\mathbb{T},0_1}$.

For small tube sizes (2×1 and 3×1 tubes), we previously [34] used exact generation to determine all smallest-span connect-sum trefoil knot patterns. (See Figures 1 and 2 for such patterns in the 2×1 tube.) Counts are shown in Table 1.

Towards exploring how the knot statistics depend on the model used (fixed-edge or fixed-span), limiting probabilities of occurrence of these smallest trefoil patterns were determined under each of the distributions $\mathbb{P}_n^{(\mathrm{ed},f)}$ $(-\infty < f < \infty,\ n \to \infty)$ and $\mathbb{P}_s^{(\mathrm{sp},g)}$ $(-\infty < g < \infty,\ s \to \infty)$. These limiting probabilities can be determined (see Lemma 1 in Section 3.2 and more generally [40]) from the eigenvalues and eigenvectors of the transfer matrix. Figure 3 shows the results for the 3×1 tube. In this figure, for the fixed-edge model ($\mathbb{P}_n^{(\mathrm{ed},f)}$), $\mathbb{P}^{\mathrm{ed}}_{3_1}(f)$ denotes the limiting $(n \to \infty)$ probability of occurrence of a smallest trefoil knot pattern at a section of a polygon. Similarly, for the fixed-span model ($\mathbb{P}_s^{(\mathrm{sp},g)}$), $\mathbb{P}^{\mathrm{sp}}_{3_1}(g)$ denotes the limiting $(s \to \infty)$ probability of occurrence of a smallest trefoil knot pattern at a section of a polygon. Further note that Figure 3 shows the results for the fixed-edge probabilities with the horizontal axis corresponding to f while for the fixed-span probabilities it corresponds to $-g$. The latter was done to make an easier comparison between the models, since positive values of f and negative values of g both have a stretching effect on polygons. Although not shown here, the observed trends were similar for the 2×1 tube. We observe that, for $\mathbb{T}_{2,1}$ and $\mathbb{T}_{3,1}$, the limiting occurrence probability of the smallest-span trefoil knot patterns decreases (resp. increases) monotonically with f (resp. g) and approaches a value slightly above the Hamiltonian polygon occurrence probability as $f \to -\infty$ (resp. $g \to \infty$). In Section 3.1 we explain that this is due to the existence of "full" trefoil knot patterns which are non-Hamiltonian.

In addition to determining smallest span trefoil patterns, exact counts were obtained for $q_{\mathbb{T},s}(K)$ and $p^{\mathrm{H}}_{\mathbb{T},(s+1)W_{\mathbb{T}}}(K)$ for some small spans s and for four different tube sizes. The method used is outlined in [40] and is based on information gained from the relevant transfer matrices. The knot-types of all polygons were determined and the resulting counts are shown in Tables 2 and 3. Counts shown for $q_{\mathbb{T},s}(K)$ have been further delineated by the number of edges n and such counts are available from the authors by request. Note that total counts for Hamiltonian polygons in 2×1, 3×1 and 2×2 tubes were published in 1998 [39, TABLE III] and our total counts for these tubes confirm the 1998 results; counts by knot-type were not considered in [39].

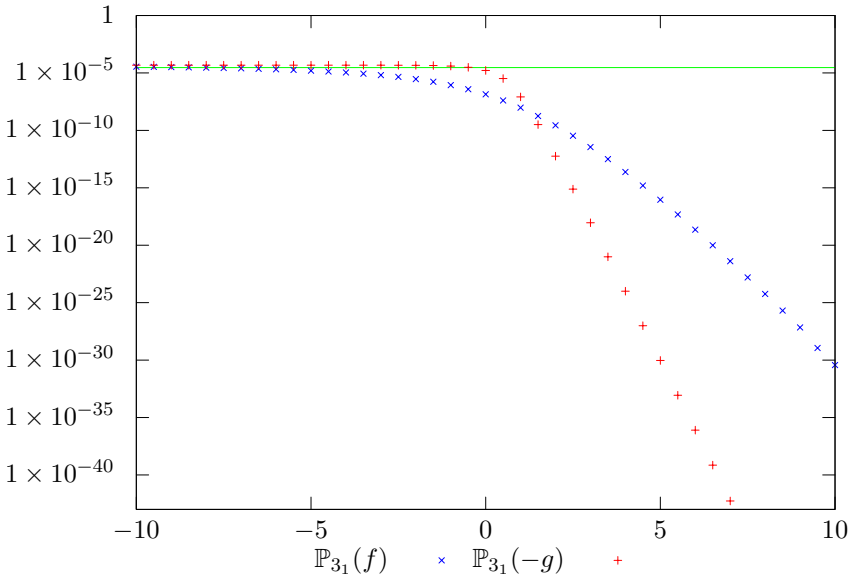

Figure 3: Log scale plot of the probabilities of the smallest trefoil patterns in the 3×1 tube, as functions of f (blue) and $-g$ (red). The horizontal line (green) denotes the limiting probability as $f \to -\infty$ of the smallest span Hamiltonian trefoil patterns.

Table 2: SAP exact generation results.

Tube	Span	Total	3_1^+	3_1^-	4_1
2×1	1	219	0	0	0
2×1	2	7,631	0	0	0
2×1	3	264,543	0	0	0
2×1	4	9,101,347	0	0	0
2×1	5	312,733,719	0	0	0
2×1	6	10,745,324,481	1,832	1,832	0
3×1	1	1,528	0	0	0
3×1	2	277,400	0	0	0
3×1	3	47,368,928	598	598	0
3×1	4	7,863,265,372	382,257	382,257	36
4×1	1	10,197	0	0	0
4×1	2	9,633,793	0	0	0
4×1	3	7,939,543,353	383,543	383,543	36
2×2	1	8,052	0	0	0
2×2	2	3,410,348	0	0	0
2×2	3	1,430,358,664	4,182	4,182	0

Table 3: Hamiltonian SAP exact generation results.

Tube	Span	Total	3_1^+	3_1^-	4_1	5_1^+	5_1^-	5_2^+	5_2^-	6_1^+	6_1^-	$3_1^+\#3_1^-$	8_{19}	8_{19}^-
2×1	1	22	0	0	0	0	0	0	0	0	0	0	0	0
2×1	2	324	0	0	0	0	0	0	0	0	0	0	0	0
2×1	3	4,580	0	0	0	0	0	0	0	0	0	0	0	0
2×1	4	64,558	0	0	0	0	0	0	0	0	0	0	0	0
2×1	5	908,452	0	0	0	0	0	0	0	0	0	0	0	0
2×1	6	12,788,368	144	144	0	0	0	0	0	0	0	0	0	0
2×1	7	180,011,762	4,302	4,302	0	0	0	0	0	0	0	0	0	0
2×1	8	2,533,935,102	96,620	96,620	72	0	0	0	0	0	0	0	0	0
3×1	1	82	0	0	0	0	0	0	0	0	0	0	0	0
3×1	2	4,580	0	0	0	0	0	0	0	0	0	0	0	0
3×1	3	232,908	58	58	0	0	0	0	0	0	0	0	0	0
3×1	4	11,636,834	5,710	5,710	16	0	0	0	0	0	0	0	0	0
3×1	5	578,377,118	458,980	458,980	3,216	32	32	70	70	2	2	36	0	0
4×1	1	306	0	0	0	0	0	0	0	0	0	0	0	0
4×1	2	64,558	0	0	0	0	0	0	0	0	0	0	0	0
4×1	3	11,636,834	5,710	5,710	16	0	0	0	0	0	0	0	0	0
4×1	4	2,040,327,632	2,264,820	2,264,820	35,816	3,148	3,148	8	8	0	0	0	4	4
2×2	1	324	0	0	0	0	0	0	0	0	0	0	0	0
2×2	2	0	0	0	0	0	0	0	0	0	0	0	0	0
2×2	3	3,918,744	96	96	0	0	0	0	0	0	0	0	0	0
2×2	4	0	0	0	0	0	0	0	0	0	0	0	0	0

Determining the knot-type of a polygon or a knot pattern requires the whole polygon or knot pattern. However, since the numbers of polygons and knot patterns in a tube grow exponentially with either span or the number of edges, exact generation has so far been limited to the cases shown in Tables 1, 2 and 3. To explore knotting statistics further, a Monte Carlo approach was developed to generate random polygons in the tube, based on a method of [43]. The Monte Carlo method is also based on transfer-matrices and can be used to generate a set of independent and identically distributed polygons from any of the distributions $\left\{\mathbb{P}_n^{(\mathrm{ed},f)}, \mathbb{P}_s^{(\mathrm{sp},g)}\right\}$ provided that the transfer matrix associated with $G_{\mathbb{T}}(f,g)$ is known. Details of the approach are given in Section 3.2. Based on the exact results of Figure 3, we focused primarily on the Hamiltonian polygon model where the probabilities of the smallest trefoil patterns were large (compared to the other models) and where the knot probabilities for small spans are also large. Similarly we focus on the 3×1 tube, since knots are far more common than in 2×1 while the transfer matrices are small enough as to make simulations and enumerations reasonably efficient.

2.4 Fixed-span vs. fixed-edge

Here we briefly make a comment about why we are focusing on the fixed-span and Hamiltonian models, instead of the fixed-edge model. Superficially, it is simply because non-trivial knots are far more common in the first two models. For example, in the 3×1 tube, we can compare the growth rates of unknots to all polygons:

$$\log\left(\frac{\mu_{\mathbb{T},0_1}}{\mu_{\mathbb{T}}}\right) \approx -1.2 \times 10^{-7} \qquad \text{(fixed-edge)} \tag{27}$$

$$\frac{1}{\langle O_{\mathbb{T}}\rangle}\log\left(\frac{\nu_{\mathbb{T},0_1}}{\nu_{\mathbb{T}}}\right) \approx -2.1 \times 10^{-5} \qquad \text{(fixed-span)} \tag{28}$$

$$\frac{1}{W_{\mathbb{T}}}\log\left(\frac{\nu^{\mathrm{H}}_{\mathbb{T},0_1}}{\nu^{\mathrm{H}}_{\mathbb{T}}}\right) \approx -8.9 \times 10^{-5} \qquad \text{(Hamiltonian)} \tag{29}$$

where $\langle O_{\mathbb{T}} \rangle$ is the average number of occupied vertices per span in the fixed-span model (see Section 4.1, (45) and (46) for further explanation of the latter two quantities). We see here that unknots are far less dominant in the fixed-span and Hamiltonian ensembles than in the fixed-edge ensemble.

Of course, this begs the question: why are knots more likely in one ensemble than another? This is because fixed-span polygons tend to be *more dense* than fixed-edge polygons, that is, the average number of edges (or equivalently, vertices) per unit span is greater for fixed-span. For example, again in the 3×1 tube, the average density of edges for a long fixed-span polygon is approximately 6.52, while for a fixed-edge polygon it is only 4.11. (Of course for a Hamiltonian polygon, it is exactly 8.) A greater density provides more opportunities for strands to get tangled, and thus leads to a higher knot probability.

Regardless of the model, we expect that conjectures analogous to those of (8) and (9) will hold and we focus on the fixed-span models for which we have been able to obtain the most data. In that regard, when K is a knot-type, the notation $\mathbb{P}_s^{(\mathrm{sp})}(K)$ ($\mathbb{P}_s^{\mathrm{H}}(K)$) will denote the probability of a polygon having knot-type K according to the fixed-span distribution $\mathbb{P}_s^{(\mathrm{sp},0)}$ ($\mathbb{P}_s^{\mathrm{H}}$) defined in Section 2.2. Then, for example, the analogue of the conjectured form (9) for these two fixed-span models is: there exist constants (independent of s) $C_{\mathbb{T},0_1}^{\mathrm{sp}}$ and $\nu_{\mathbb{T},0_1}$ such that,

$$q_{\mathbb{T},s}(0_1) \sim C_{\mathbb{T},0_1}^{(\mathrm{sp})} (\nu_{\mathbb{T},0_1})^s, \qquad \text{as} \quad s \to \infty; \tag{30}$$

and for Hamiltonian polygons, there exist constants (independent of s) $C_{\mathbb{T},0_1}^{\mathrm{H}}$ and $\nu_{\mathbb{T},0_1}^{\mathrm{H}}$ such that,

$$p_{\mathbb{T},(s+1)W_{\mathbb{T}}}^{\mathrm{H}}(0_1) \sim C_{\mathbb{T},0_1}^{\mathrm{H}} (\nu_{\mathbb{T},0_1}^{\mathrm{H}})^s, \qquad \text{as} \quad s \to \infty. \tag{31}$$

3 Numerical approaches and transfer matrix methods

We first review the transfer matrix method and then sketch the Monte Carlo approach used to randomly sample self-avoiding polygons and Hamiltonian polygons in a tube $\mathbb{T}$.

3.1 Transfer matrix method

We rely on the definitions for start, proper and end *1-pattern* for polygons as given in [36]; essentially these are sets of edges and vertices that can occur between two consecutive half-integer x-planes in a polygon in $\mathbb{T}$ along with a pair partition which defines how any endpoints in the first half-integer plane are connected up on the left within a polygon. By dividing up a polygon with span s at each half-integer x-plane (starting at $x = -1/2$ and ending at $x = s + 1/2$), a polygon can then be thought of as a sequence of $(s+1)$ 1-patterns that starts with a start 1-pattern, followed by $s-1$ proper 1-patterns, and then ends with an end 1-pattern. We then say a given 1-pattern q can follow another 1-pattern p if q can occur immediately to the right of p in some polygon in $\mathbb{T}$. Given an ordering of all proper 1-patterns, we can then define the transfer matrix $\mathbf{M}$ for polygons in $\mathbb{T}$ as:

$$\mathbf{M}_{ij}(g) = \begin{cases} e^{g|j|}, & \text{if the } j^{\text{th}} \text{ 1-pattern can follow the } i^{\text{th}} \text{ 1-pattern} \\ 0, & \text{otherwise,} \end{cases} \tag{32}$$

where $|j|$ is the number of polygon edges (1/2 edges contribute 1/2) in the j^{th} 1-pattern. We can similarly define a start (end) transfer matrix which has a non-zero entry $\mathbf{S}_{ij}(g) = e^{g(|i|+|j|)}$ ($\mathbf{E}_{ij}(g) = e^{g|j|}$) when the j^{th} proper 1-pattern can follow the i^{th} start 1-pattern (when the j^{th} end 1-pattern can follow the i^{th} proper 1-pattern).

Using these matrices, the grand-canonical partition function introduced in the last section can now be written as:

$$\begin{aligned} G_{\mathbb{T}}(f,g) &= \sum_{s\geq 0}\sum_{n\geq 4} p_{\mathbb{T},n}(s)e^{gn+fs} \\ &= \left[\sum_{s=0}^{1}\sum_{n\geq 4} p_{\mathbb{T},n}(s)e^{gn+fs}\right] + \sum_{i,j}\left[\sum_{k\geq 0} e^{f(k+2)}\mathbf{S}(g)\mathbf{M}(g)^k\mathbf{E}(g)\right]_{i,j} \\ &= \left[\sum_{s=0}^{1}\sum_{n\geq 4} p_{\mathbb{T},n}(s)e^{gn+fs}\right] + e^{2f}\sum_{i,j}\left[\mathbf{S}(g)(\mathbf{I}-e^{f}\mathbf{M}(g))^{-1}\mathbf{E}(g)\right]_{i,j}, \end{aligned} \tag{33}$$

where the sum over i,j is over all start 1-patterns (i) and end 1-patterns (j). Note that for a fixed f or g, the radius of convergence of this partition function is determined by the singularities of $\det(\mathbf{I}-e^{f}\mathbf{M}(g))$ and hence the eigenvalues of $\mathbf{M}(g)$. This in turn can be used to determine the limiting free energies defined in the last section. Specifically, to determine the fixed-edge model limiting free energy for a given force f, set $x=e^{g}$ and let $R^{\mathrm{ed}}(f)$ denote the radius of convergence of $G_{\mathbb{T}}(f,g)$ as a power series in x, then

$$\mathcal{F}_{\mathbb{T}}(f) = \lim_{n\to\infty}\frac{1}{n}\log Z_{\mathbb{T},n}(f) = -\log R^{\mathrm{ed}}(f). \tag{34}$$

Similarly, to determine the fixed-span model limiting free energy for a given value for g, set $y=e^{f}$ and let $R^{\mathrm{sp}}(g)$ denote the radius of convergence of $G_{\mathbb{T}}(f,g)$ as a power series in y, then

$$\mathcal{G}_{\mathbb{T}}(g) = \lim_{s\to\infty}\frac{1}{s}\log Q_{\mathbb{T},s}(g) = -\log R^{\mathrm{sp}}(g). \tag{35}$$

More generally, [36] also define s-patterns to be sets of edges and vertices that can occur between two half-integer x-planes, $x=k+1/2$ and $x=s+k+1/2$, in a polygon in $\mathbb{T}$ along with a pair partition which defines how any endpoints in the first half-integer plane ($x=k+1/2$) are connected up on the left within a polygon. The span of an s-pattern is thus s. Any s-pattern which consists of $(s-1)W$ vertices is called *full* and if it can also occur in a Hamiltonian polygon then it is called a Hamiltonian pattern. While every Hamiltonian pattern is necessarily full, not every full pattern is a Hamiltonian pattern.

In general it is not possible to assign a knot type to an s-pattern, as there may be many ways to connect up the "loose ends" on the left and right. The exception is when an s-pattern is also a connect-sum pattern; in that case there is only one way to join the ends. Table 1 focuses on connect-sum patterns whose knot type is a trefoil – it shows the number of full connect sum trefoil patterns (last column) along with the number of those which are Hamiltonian for various spans.

By restricting the transfer matrix defined above to either proper full or proper Hamiltonian 1-patterns, one can obtain transfer matrices $\mathbf{M}^{\mathrm{F}}$ and $\mathbf{M}^{\mathrm{H}}$ for full patterns and Hamiltonian polygons, respectively, and from their spectra determine:

$$\beta^{\mathrm{F}}_{\mathbb{T}} \equiv \lim_{s\to\infty} s^{-1}\log t^{\mathrm{F}}_{\mathbb{T},s}, \tag{36}$$

$$\kappa^{\mathrm{H}}_{\mathbb{T}} \equiv \lim_{s\to\infty}\frac{1}{(s+1)W_{\mathbb{T}}}\log p^{\mathrm{H}}_{\mathbb{T},(s+1)W_{\mathbb{T}}}, \tag{37}$$

where $t^{\mathrm{F}}_{\mathbb{T},s}$ is the number of full s-patterns. In [36] it was established that $\beta^{\mathrm{F}}_{\mathbb{T}}/W_{\mathbb{T}} = \kappa^{\mathrm{H}}_{\mathbb{T}}$ for all tubes such that $5\geq L\geq M\geq 0$; this is because Hamiltonian s-patterns are the dominant

class amongst full s-patterns. It is also known that for any tube dimensions $\lim_{f\to-\infty}\mathcal{F}_{\mathbb{T}}(f) = \beta^{\mathrm{F}}_{\mathbb{T}}/W_{\mathbb{T}}$. However, because for any finite f one expects that there will always be a non-zero probability that a non-Hamiltonian full s-pattern occurs, we expect that the probability of, for example, full connect-sum trefoil patterns will be greater than that for Hamiltonian connect-sum trefoil patterns for every finite $f > -\infty$. We see this in Figure 3 where the horizontal line corresponds to the probability of the Hamiltonian trefoil patterns occurring in a Hamiltonian polygon.

3.2 Monte Carlo method

Next we briefly sketch the method used to randomly sample self-avoiding polygons and Hamiltonian polygons in a tube $\mathbb{T}$. The polygons are sampled uniformly at random from either the fixed-length or fixed-span ensembles. (Note that for Hamiltonian polygons, length determines span, so that these two ensembles are equivalent.) Any two samples are independent, so there is no need to account for correlations.

The method is inspired by one proposed in [43], but we make some modifications here. The approach will work for any of the three models (fixed-edge, fixed-span or Hamiltonian polygons). For the fixed-edge model take $f = 0$ and $x = e^g$ in (33) and set $\mathbf{M} \equiv \mathbf{M}(\log(x))$; in this case each n-edge polygon in $\mathbb{T}$ is considered to be equally likely (uniform). For a given value of x let $\rho(x)$ be the spectral radius of $\mathbf{M}$, and let x_0 be the smallest positive real value of x which makes $\rho(x) = 1$. The Perron-Frobenius theorem implies that such a value exists, and moreover that at $x = x_0$, 1 will be a simple eigenvalue[1] of $\mathbf{M}$. Let ξ (resp. η) be the right (resp. left) eigenvector corresponding to that eigenvalue. Then we have the following lemma for the fixed-edge ensemble.

Lemma 1 (Alm and Janson [43])**.** *Let i and j represent proper 1-patterns such that j can follow i. Let $\mathsf{p}^{\mathrm{ed}}_{ij}(n)$ be the probability that an occurrence of i in a uniformly random polygon of length n is followed by j. Then as $n \to \infty$,*

$$\mathsf{p}^{\mathrm{ed}}_{ij}(n) \to \mathsf{p}^{\mathrm{ed}}_{ij} = x_0^{|j|}\frac{\xi_j}{\xi_i}. \tag{38}$$

Furthermore, for any polygon pattern P consisting of a sequence of b internal 1-patterns $\pi_1, \ldots, \pi_b$, the probability, $\mathsf{p}^{\mathrm{ed}}_P(n)$, that P occurs at any given section of a random length-n polygon satisfies (as $n \to \infty$):

$$\begin{aligned}\mathsf{p}^{\mathrm{ed}}_P(n) \to \mathsf{p}^{\mathrm{ed}}_P &= (\eta_{\pi_1}\xi_{\pi_1})\left(x_0^{|\pi_2|}\frac{\xi_{\pi_2}}{\xi_{\pi_1}}\right)\left(x_0^{|\pi_3|}\frac{\xi_{\pi_3}}{\xi_{\pi_2}}\right)\cdots\left(x_0^{|\pi_b|}\frac{\xi_{\pi_b}}{\xi_{\pi_{b-1}}}\right)\\ &= \eta_{\pi_1}x_0^{|\pi_2|+|\pi_3|+\cdots+|\pi_b|}\xi_{\pi_b},\end{aligned} \tag{39}$$

where $|\pi_i|$ denotes the number of edges of the 1-pattern.

For the fixed-span ensemble with $g = 0$ (the probability of each span s polygon is equally likely), the above result requires only minor modification. Let λ be the dominant eigenvalue of $\mathbf{M}(0)$. By the Perron-Frobenius theorem, λ is real, positive and simple. Let ζ be the corresponding right eigenvector.

Lemma 2. *Let i and j represent proper 1-patterns such that j can follow i. Let $\mathsf{p}^{\mathrm{sp}}_{ij}(s)$ be the probability that an occurrence of i in a uniformly random polygon of span s is followed by j. Then as $s \to \infty$,*

$$\mathsf{p}^{\mathrm{sp}}_{ij}(s) \to \mathsf{p}^{\mathrm{sp}}_{ij} = \lambda^{-1}\frac{\zeta_j}{\zeta_i}. \tag{40}$$

[1] This requires that $\mathbf{M}$ be irreducible, which can be demonstrated by a straightforward concatenation argument for polygons (see for example [41]).

We randomly generate polygons by building them one 1-pattern at a time, using Lemmas 1 and 2 to inform our choice of transition probabilities. For the fixed-span ensemble with $g = 0$, the procedure for generating a polygon π, comprised of 1-patterns $\pi_0, \pi_1, \ldots, \pi_s$, is as follows.

1. π_0 is selected uniformly at random from all S start 1-patterns.
2. With probability $r_1(\pi_0)$ (detailed below), the sample is rejected and we return to step 1. Otherwise, π_1 is selected from all proper 1-patterns which can follow π_0 with probability proportional to ζ_{π_1}.
3. For $i = 2, 3, \ldots, s-1$, choose π_i with probability $\mathsf{p}^{\mathrm{sp}}_{\pi_{i-1},\pi_i}$.
4. With probability $r_s(\pi_{s-1})$ (detailed below), the sample is rejected and we return to step 1. Otherwise, π_s is selected uniformly from all end 1-patterns which can follow π_{s-1}.

The probabilities r_1 and r_s are chosen so as to make the sampling uniformly random. First define

$$t_1(i) = \sum_{\substack{j \text{ proper} \\ j \text{ follows } i}} \zeta_j \quad \text{and} \quad t_s(i) = \frac{\#\text{ end 1-patterns following } i}{\zeta_i}. \tag{41}$$

Then

$$r_1(\pi_0) = 1 - \frac{t_1(\pi_0)}{\max\limits_{i \text{ start}} \{t_1(i)\}} \quad \text{and} \quad r_s(\pi_{s-1}) = 1 - \frac{t_s(\pi_{s-1})}{\max\limits_{i \text{ proper}} \{t_s(i)\}}. \tag{42}$$

Sampling from the fixed-edge ensemble (with $f = 0$) works in a similar way, with the main difference being that the procedure is terminated once the polygon length (rather than the span) reaches the desired value.

3.3 Determining the knot type

A standard technique for determining the knot type of a polygon is to take a projection of the polygon and compute a polynomial invariant, like the Alexander or HOMFLY polynomial. While this does not perfectly distinguish between different knot types (some knots have the same polynomials), such "collisions" are expected to be rare for the size of polygons studied here (where the most likely prime knots have small minimum crossing number) and hence they are unlikely to noticeably affect any statistics.

As will be seen in the next section, polygons of span s in narrow tubes are dominated by unknots until s gets into the thousands. However, the projection of such a large polygon (even an unknot) will contain many hundreds or thousands of crossings. This makes the direct computation of any knot polynomial prohibitively difficult.

Instead, we employ two techniques to simplify this procedure. Firstly, we make use of the aforementioned 2-sections. Wherever a polygon of knot type K contains a 2-section, one can cut it into two pieces, close up the loose ends to form two smaller polygons of knot types K_1 and K_2, and know that $K = K_1 \# K_2$. By repeating this procedure, a long polygon can be split into a sequence of p smaller polygons, with $K = K_1 \# K_2 \# \ldots \# K_p$. Moreover, the pattern theorems for polygons in $\mathbb{T}$ imply that long polygons have a positive density of 2-sections, so on average $p = O(s)$. Each of these smaller polygons will have far fewer crossings than the original.

Secondly, we make use of the fact that any polygon on the cubic lattice with length less than 24 is an unknot [44]. If any of the small polygons obtained during the "cutting" procedure have length 22 or smaller, they are unknots and can immediately be discarded. For those pieces of length 24 or greater, we then apply the BFACF algorithm (see [45] and references therein) in an attempt to decrease the size without changing the knot type. BFACF is a Monte Carlo

procedure that involves making "local moves" to transform a polygon; here we are not using it as a Monte Carlo tool, but rather taking advantage of the fact that (a) it does not change the knot type, and (b) it can be modified to preferentially decrease the size of polygons. If the size drops below 24, we can again discard the piece. (Note that while the original polygon was confined to the tube, when applying BFACF we no longer need the tube restriction.)

After cutting up the polygon and shrinking its constituent pieces as much as possible, we are left with a sequence of sub-polygons of lengths ≥ 24 and indeterminate knot type. These are then loaded into KnotPlot [46], which algorithmically determines the knot type following an approach which is detailed in [47].

4 Results

4.1 Growth constants

For the remainder of this paper we will focus on the fixed-span and Hamiltonian models in the tube, and for fixed-span set $g = 0$ (i.e. no stretching or compressing force). We first consider the growth rates of all polygons. As mentioned in the previous section, these can be determined directly from the transfer matrix, if it is known. The results for the 2×1 and 3×1 tubes are presented in Table 4.

Table 4: Growth rates for all and Hamiltonian polygons in the 2×1 and 3×1 tubes, counted by span. For all values the error is numerical and expected to be confined to the last digit.

Tube Size	$\chi_{\mathbb{T}}$	$\nu_{\mathbb{T}}$	$\chi^{\mathrm{H}}_{\mathbb{T}}$	$\nu^{\mathrm{H}}_{\mathbb{T}}$
2×1	3.53689835537159142	34.3601806741352594	2.644502344846937	14.07643812777425
3×1	5.10696921077147344	165.1690030762774319	3.904865602438742	49.643407510907971

We note here that, since $\nu_{\mathbb{T}}$ and $\nu^{\mathrm{H}}_{\mathbb{T}}$ are eigenvalues of matrices with integer entries, they are algebraic numbers. However, we have no reason to expect their minimal polynomials to be of low degree, and indeed would expect such polynomials to quickly increase in complexity as tube size grows.

For Hamiltonian polygons in the 2×1 tube, in Figure 4(a) we use our Monte Carlo generated data and plot statistical estimates for $\log \mathbb{P}^{\mathrm{H}}_{s}(0_1)$ against s (span), together with a linear best fit.

As is clear from the plot, the linear fit is very good. We therefore can conclude that $\log \mathbb{P}^{\mathrm{H}}_{\mathbb{T},s}(0_1) \sim as + b$, where $a = -2.86675 \times 10^{-5} \pm 2.285 \times 10^{-8}$ and $b = 1.79821 \times 10^{-4} \pm 7.813 \times 10^{-7}$, where the error bars denote the asymptotic standard error reported by gnuplot [48] using a weighted least squares fit. Note that there is no need for a power-law correction as per (5). We therefore expect the form

$$\log \mathbb{P}^{\mathrm{H}}_{\mathbb{T},s}(0_1) \sim C + s \log \left(\frac{\nu^{\mathrm{H}}_{\mathbb{T},0_1}}{\nu^{\mathrm{H}}_{\mathbb{T}}} \right), \qquad s \to \infty, \tag{43}$$

for a constant C, and it follows that $\nu^{\mathrm{H}}_{\mathbb{T},0_1} = 14.0760346$, with errors confined to the last digit. This provides evidence that the analogue of the conjectured form (9) for Hamiltonian polygons holds in the 2×1 tube, i.e. that the form (31) is correct.

We repeat this procedure for all polygons in the 2×1 tube, as well as Hamiltonian and all polygons in 3×1 – see Figures 4(b), 5(a) and 5(b). In each case we have a very good linear fit, providing further evidence that the analogues of the asymptotic form (9) (namely (30) and (31))

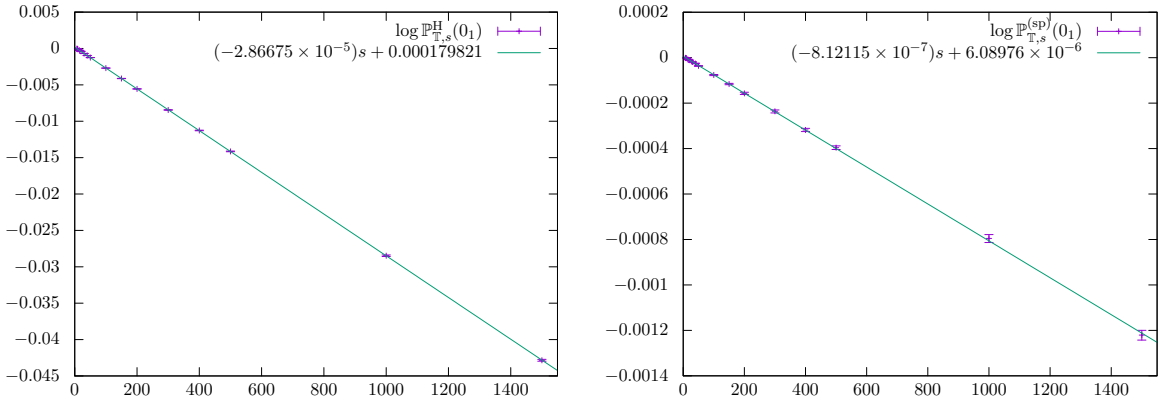

(a) **(b)**

Figure 4: Plots of (a) $\log \mathbb{P}^{\mathrm{H}}_{\mathbb{T},s}(0_1)$ and (b) $\log \mathbb{P}^{(\mathrm{sp})}_{\mathbb{T},s}(0_1)$ against s (span) for the $\mathbb{T} = 2 \times 1$ tube, together with linear best fits. Error bars indicate 95% confidence intervals.

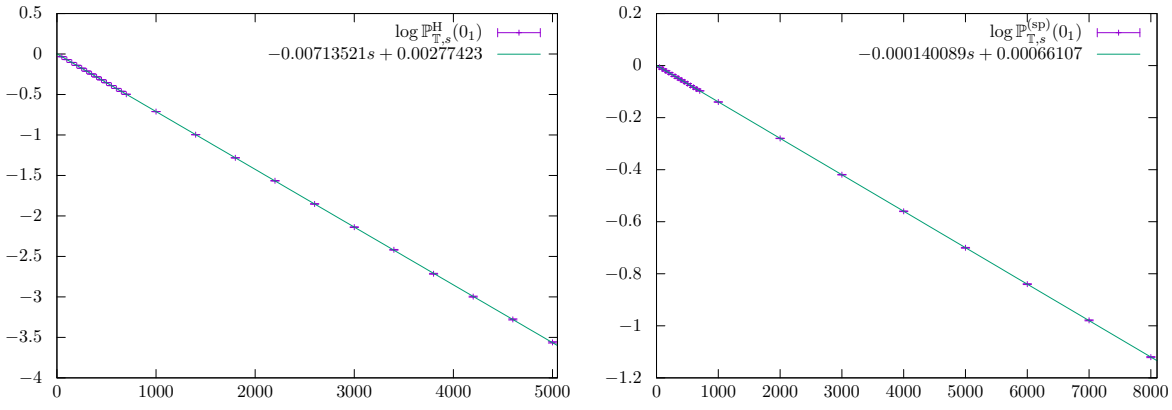

(a) **(b)**

Figure 5: Plots of (a) $\log \mathbb{P}^{\mathrm{H}}_{\mathbb{T},s}(0_1)$ and (b) $\log \mathbb{P}^{(\mathrm{sp})}_{\mathbb{T},s}(0_1)$ against s (span) for the $\mathbb{T} = 3 \times 1$ tube, together with linear best fits. Error bars indicate 95% confidence intervals.

hold. The results for the growth rates of unknotted polygons in all four cases are summarised in Table 5.

Table 5: Statistically estimated growth rates for all and Hamiltonian unknotted polygons in the 2×1 and 3×1 tubes, counted by span. Standard errors are expected to be confined to the last digit.

Tube Size	$\nu_{\mathbb{T},0_1}$	$\nu^{\mathrm{H}}_{\mathbb{T},0_1}$
2×1	34.3601527	14.0760346
3×1	165.14587	49.60800

Note that unlike $\nu_{\mathbb{T}}$ and $\nu^{\mathrm{H}}_{\mathbb{T}}$, it is unknown if $\nu_{\mathbb{T},0_1}$ or $\nu^{\mathrm{H}}_{\mathbb{T},0_1}$ are algebraic numbers.

These results should be compared to the best estimates for the unrestricted cubic lattice $\mathbb{Z}^3$. There, it is estimated [19] that

$$\log\left(\frac{\mu_{0_1}}{\mu}\right) = (-4.15 \pm 0.32) \times 10^{-6}. \tag{44}$$

The figures given in Tables 4 and 5 are for polygons counted by span, not length; however, as previously observed, for Hamiltonian polygons these are in direct proportion. Using (19), we find

$$\log\left(\frac{\mu^{\mathrm{H}}_{\mathbb{T},0_1}}{\mu^{\mathrm{H}}_{\mathbb{T}}}\right) = \frac{1}{W_{\mathbb{T}}} \log\left(\frac{\nu^{\mathrm{H}}_{\mathbb{T},0_1}}{\nu^{\mathrm{H}}_{\mathbb{T}}}\right) \approx \begin{cases} -4.78 \times 10^{-6} & \mathbb{T} = 2 \times 1 \text{ tube} \\ -8.92 \times 10^{-5} & \mathbb{T} = 3 \times 1 \text{ tube.} \end{cases} \tag{45}$$

That is, knots in Hamiltonian polygons in the 2×1 and 3×1 tubes are more common than they are in all polygons on the cubic lattice.

For all polygons in the fixed-span ensemble, the lengths of polygons are not fixed and therefore there is no exact way to make a direct comparison with polygons in the full lattice. However, we can use an approximation based on (45), replacing $W_{\mathbb{T}}$ – the number of occupied vertices per unit span for Hamiltonian polygons – with the corresponding *average* $\langle O_{\mathbb{T}} \rangle$ for all polygons. As polygon size gets large, this average can be computed using the stationary distribution of the Markov chain with transition probabilities given by (40).

For the 2×1 and 3×1 tubes, these average vertex densities $\langle O_{\mathbb{T}} \rangle$ are 4.8865 and 6.5244 respectively. The analogous version of (45) is then

$$\frac{1}{\langle O_{\mathbb{T}} \rangle} \log\left(\frac{\nu_{\mathbb{T},0_1}}{\nu_{\mathbb{T}}}\right) \approx \begin{cases} -1.66 \times 10^{-7} & \mathbb{T} = 2 \times 1 \text{ tube} \\ -2.147 \times 10^{-5} & \mathbb{T} = 3 \times 1 \text{ tube.} \end{cases} \tag{46}$$

Using this rough approximation, we see that knots in the 2×1 tube are less likely than in the cubic lattice, but more likely in the 3×1 tube.

Having provided strong evidence that

$$\mathbb{P}^{(\mathrm{sp})}_{\mathbb{T},s}(0_1) \sim A^{(\mathrm{sp})}_{\mathbb{T}} \left(\frac{\nu_{\mathbb{T},0_1}}{\nu_{\mathbb{T}}}\right)^s \qquad \text{and} \qquad \mathbb{P}^{\mathrm{H}}_{\mathbb{T},s}(0_1) \sim A^{\mathrm{H}}_{\mathbb{T}} \left(\frac{\nu^{\mathrm{H}}_{\mathbb{T},0_1}}{\nu^{\mathrm{H}}_{\mathbb{T}}}\right)^s, \tag{47}$$

we can see that for $K = 0_1$, the asymptotic form (4) does indeed appear to hold, with $\Delta N(0_1) \approx 0$. We now wish to investigate if this is still the case with other knot types. That is, we investigate whether the analogue of the conjectured form (8) holds.

In Figures 6 and 7 we plot the probabilities of various prime knot types divided by the probability of the unknot, scaled by constant factors so as to be visible in the same plot. The very clear linear form of all these plots (except for some numerical uncertainty at large lengths

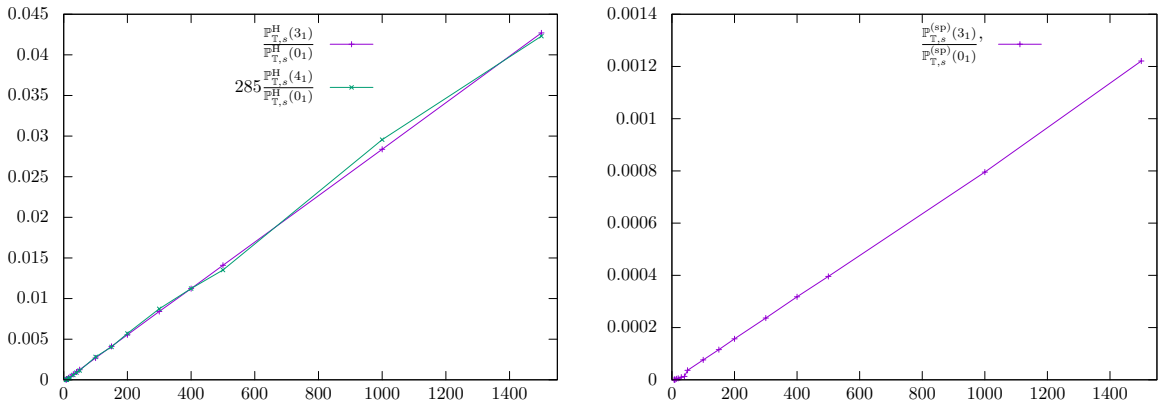

(a) **(b)**

Figure 6: For the 2×1 tube: (a) Plots of $\mathbb{P}^{\mathrm{H}}_{\mathbb{T},s}(3_1)/\mathbb{P}^{\mathrm{H}}_{\mathbb{T},s}(0_1)$ and $\mathbb{P}^{\mathrm{H}}_{\mathbb{T},s}(4_1)/\mathbb{P}^{\mathrm{H}}_{\mathbb{T},s}(0_1)$, with the latter scaled by a constant factor for clarity, against s (span); (b) A plot of $\mathbb{P}^{(\mathrm{sp})}_{\mathbb{T},s}(3_1)/\mathbb{P}^{(\mathrm{sp})}_{\mathbb{T},s}(0_1)$ against s (span).

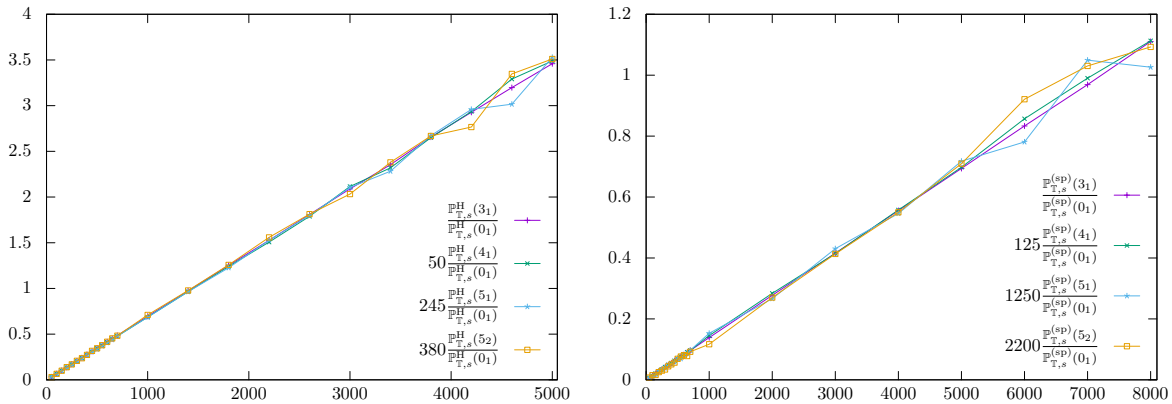

(a) **(b)**

Figure 7: For the 3×1 tube: (a) Plots of $\mathbb{P}^{\mathrm{H}}_{\mathbb{T},s}(K)/\mathbb{P}^{\mathrm{H}}_{\mathbb{T},s}(0_1)$ for $K = 3_1, 4_1, 5_1$ and 5_2, scaled by constant factors for clarity, against s (span); (b) The corresponding plots for all polygons in the fixed-span model.

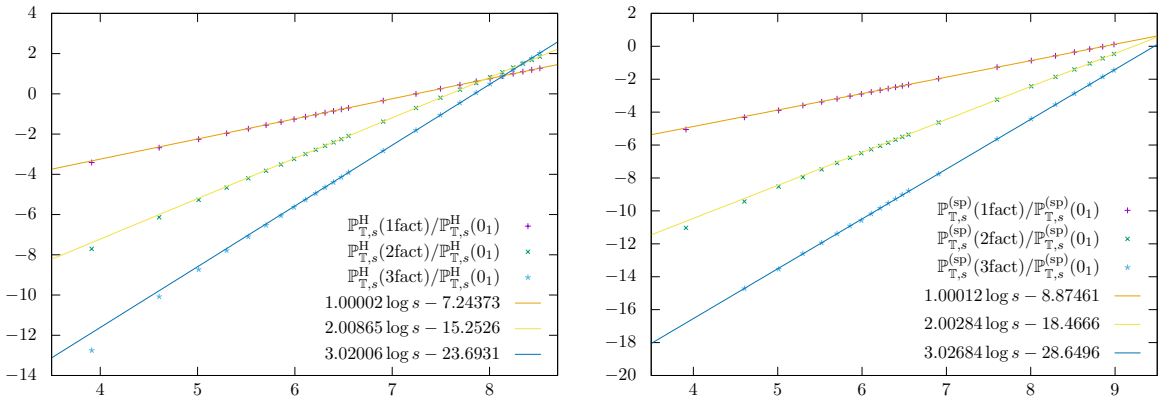

Figure 8: For the 3×1 tube: (a) Log-log plots of $\mathbb{P}^{\mathrm{H}}_{\mathbb{T},s}(k \text{ factor knot})/\mathbb{P}^{\mathrm{H}}_{\mathbb{T},s}(0_1)$, for $k = 1, 2, 3$, together with straight line fits to the last few points (spans $s \geq 1000$); (b) The corresponding plots for all polygons in the fixed-span model.

for the 5-crossing knots) confirms that (4) remains applicable for different prime knot types, with $\Delta N(K) \approx 0$ in all cases.

Figure 8 shows log-log plots of the probabilities of 1-, 2- and 3-factor knots[2], again divided by the probability of the unknot. For each we also include a straight-line fit to the last few points (spans ≥ 1000). Note that for $k = 1, 2, 3$, the slope of the line for the k-factor knots is very close to k – a further confirmation of the correctness of (4).

4.2 Further evidence related to entropic exponents

With the supposition that (based on the evidence from the previous section)

$$\mathbb{P}^{(\mathrm{sp})}_{\mathbb{T},s}(K) = A^{(\mathrm{sp})}_{\mathbb{T},K} s^{f_K} \left(\frac{\nu_{\mathbb{T},0_1}}{\nu_{\mathbb{T}}}\right)^s (1 + o(1)) \tag{48}$$

for a constant $A^{(\mathrm{sp})}_{\mathbb{T},K}$, we note that this quantity has a maximum at approximately

$$s \approx M_{\mathbb{T}}(K) \equiv -\frac{f_K}{\log\left(\frac{\nu_{\mathbb{T},0_1}}{\nu_{\mathbb{T}}}\right)}. \tag{49}$$

(The exact location can depend on the $o(1)$ term since, for example, there are knot-types K with minimum span in $\mathbb{T}$ greater than $M_{\mathbb{T}}(K)$.) An analogous form holds for Hamiltonian polygons. Note that $M_{\mathbb{T}}(K)$ does not depend on the exact knot-type of K, only the number of prime knots in its decomposition. For the four models we focus on here, an approximate value for this location is given in Table 6.

We have not attempted to sample polygons of sufficient span in the 2×1 tube to test the validity of the values given in Table 6. For the 3×1 tube, however, sufficiently long polygons have been generated to observe the maximum for $K = 1$ (all polygons) and $K = 1, 2, 3$ (Hamiltonian polygons). See Figures 9–11.

[2]The "factors" are knots identified as prime by KnotPlot (in this case, KnotPlot identifies knots up to 10 crossings), as well as knots that KnotPlot could not identify. The latter cases were exceedingly rare – on the order of 1 in 10^5 polygons for Hamiltonian polygons of span 5000, and none at all for the non-Hamiltonian polygons sampled here – and so any incorrect classifications are thus completely indiscernible in Figures 8 and 11.

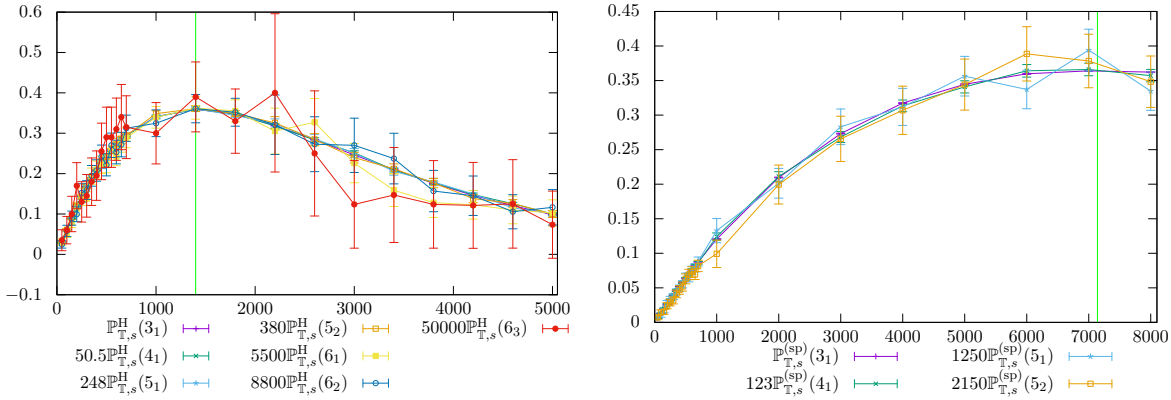

(a) **(b)**

Figure 9: Plots of (a) $\mathbb{P}^{\mathrm{H}}_{\mathbb{T},s}(K)$ and (b) $\mathbb{P}^{(\mathrm{sp})}_{\mathbb{T},s}(K)$ against s (span) for various prime knot types K in the 3×1 tube, scaled by constant factors. The vertical lines at (a) $s = 1400$ and (b) $s = 7140$ indicate the predicted locations of the maxima, as per Table 6. Error bars indicate 95% confidence intervals.

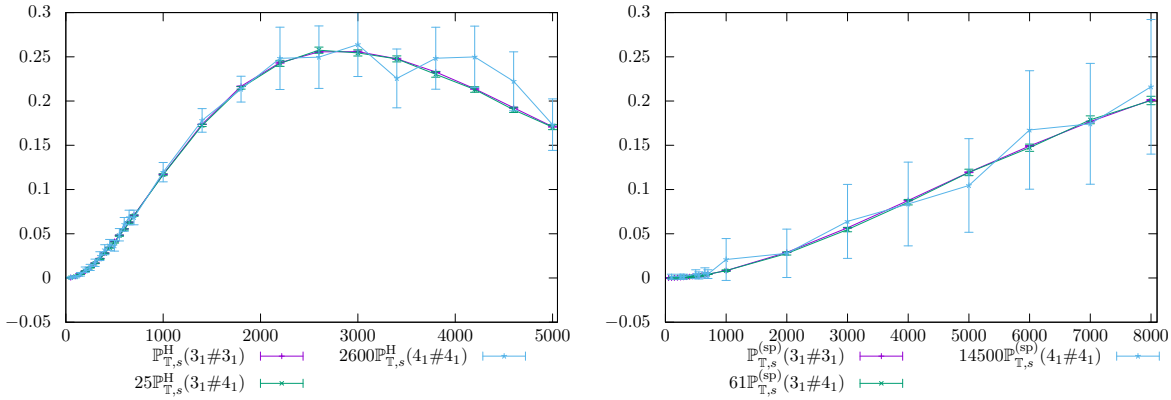

(a) **(b)**

Figure 10: Plots of (a) $\mathbb{P}^{\mathrm{H}}_{\mathbb{T},s}(K)$ and (b) $\mathbb{P}^{(\mathrm{sp})}_{\mathbb{T},s}(K)$ against s (span) for various 2-factor knot types K in the 3×1 tube, scaled by constants. Error bars indicate 95% confidence intervals.

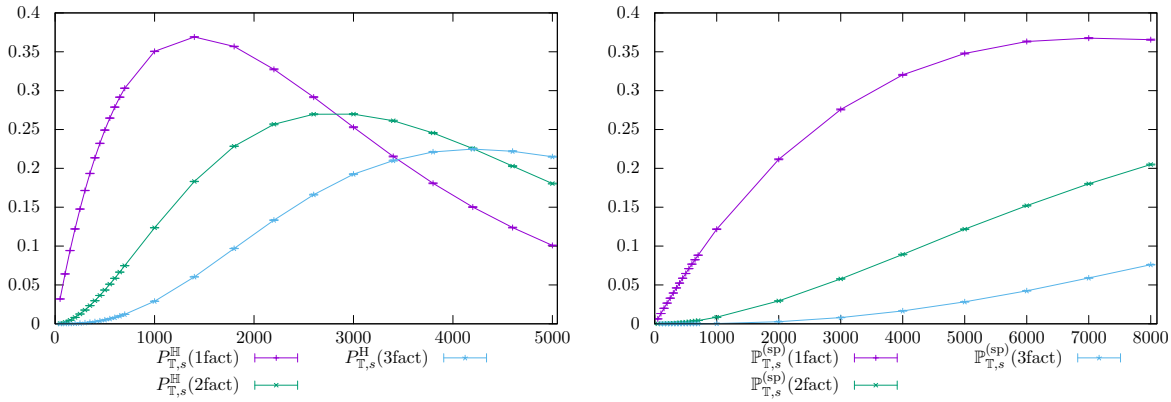

(a) **(b)**

Figure 11: Plots of (a) $\mathbb{P}^{\mathrm{H}}_{\mathbb{T},s}(k$ factor knot) and (b) $\mathbb{P}^{(\mathrm{sp})}_{\mathbb{T},s}(k$ factor knot) against s (span) for $k = 1, 2, 3$ in the 3×1 tube. Error bars indicate 95% confidence intervals.

Table 6: Approximate values for $M_{\mathbb{T}}(K)$ and $M_{\mathbb{T}}^{\mathrm{H}}(K)$, expected to be accurate to 2 or 3 significant figures.

Tube Size	$M_{\mathbb{T}}(K)$	$M_{\mathbb{T}}^{\mathrm{H}}(K)$
2×1	$(1.23 \times 10^6) f_K$	$34900 f_K$
3×1	$7140 f_K$	$1400 f_K$

4.3 Amplitude ratios

We now briefly turn our attention to amplitude ratios for prime knot types. As mentioned in Section 1, it is believed that the ratio C_K/C_{3_1} (recall (2)) is universal, and does not depend on the lattice in question.

This cannot however be true when restricted to finite-size tubes, since for any given L, M there will be infinitely many prime knot types K which cannot be embedded in the $L \times M$ tube, so $C_K = 0$. (Indeed in [49] it has been established that only knots whose trunk is less than $(L+1)(M+1)$ are embeddable in an $L \times M$ tube.) This does however also suggest that even in tubes where knots of type K can be embedded, we should not expect amplitude ratios to be universal, either between different tube sizes or between tubes and the full lattice.

To confirm this, in Table 7 we give some estimated amplitude ratios for a few different knot types in the 2×1 and 3×1 tubes, for both all and Hamiltonian polygons, as well as estimates from [20] for the full lattice.

Table 7: Estimates of amplitude ratios for 4- and 5-crossing prime knots in tubes. Insufficient data was available for useful estimates for all polygons in the 2×1 tube. Also included are estimates for the full lattice from [20]. Errors are expected to be confined to the last digit, but these relatively crude estimates are intended only for illustrative purposes.

Model	C_{4_1}/C_{3_1}	C_{5_1}/C_{3_1}	C_{5_2}/C_{3_1}
2×1 Ham.	0.0035	0.00011	8×10^{-5}
3×1 Ham.	0.020	0.0040	0.0026
3×1	0.008	0.0008	0.00045
Full lattice	0.036	0.0025	0.0036

It seems reasonable to expect that as tube size increases, the amplitude ratios for knots in the tube, sampled from the fixed-edge ensemble, should approach the full lattice values. However, it is unclear what we should expect in the limit for the fixed-span or Hamiltonian ensembles.

5 Conclusion

In this paper we have studied a model of self-avoiding polygons confined to a $L \times M$ tube of the cubic lattice $\mathbb{Z}^3$, and in particular considered the knotting properties of these polygons. This model is more tractable than that of polygons in the full lattice $\mathbb{Z}^3$, because it is characterised by a finite transfer matrix. Such a matrix characterisation allows, for example, to compute the generating function, growth rate and critical exponent for polygons in the tube. We have primarily focused on two particular ensembles of polygons: those enumerated by their span in the direction of the axis of the tube, and Hamiltonian polygons, which visit every vertex in an $L \times M \times s$ prism. This is primarily because knots are more common in these ensembles than for polygons enumerated by length.

However, polygons of fixed knot type (for example, unknots) cannot be characterised by a

finite transfer matrix. For this reason we have developed a Monte Carlo algorithm for sampling random polygons directly from a chosen Boltzmann distribution. Using this algorithm we have been able to accurately estimate the growth rate for unknots and empirically confirm that the critical exponent for a given knot type K corresponds to the number of prime factors in the knot decomposition of K. We have also estimated the sizes at which k-factor knots are most likely to occur, and verified these values using the Monte Carlo method. Finally, we have investigated amplitude ratios for given knot types in the tubes, and observed that these differ from those values (conjectured to be universal) in the full lattice.

The Monte Carlo method presented here has the distinct advantage over many other commonly used algorithms (e.g. PERM, GAS, Wang-Landau, multiple Markov chain) in that it generates completely independent samples directly from the desired Boltzmann distribution. However, it also has a significant drawback – the transfer matrix must be computed first, and must be held in memory during computation. Because the size of the transfer matrix grows extremely quickly with the size of the tube, this limits the method to only very small tube sizes.

Because polygons can be grown one "slice" at a time, a growth algorithm like PERM could be employed for this model. We are currently investigating this and other sampling methods.

As mentioned in Section 1, another work by the authors and collaborators [35] is in preparation. This focuses exclusively on polygons in the 2×1 tube, and rigorously establishes (7), i.e. that the growth rates (counting by length) of certain knot types (2-bridge knots with unknotting number one, or connect sums thereof) are the same as that of the unknot, and moreover, the exponents of such polygon knots are indeed equal to the number of prime factors in the knot decompositions.

Acknowledgements

NRB was supported by the PIMS Collaborative Research Group in Applied Combinatorics, and the Australian Research Council grant DE170100186. CES acknowledges support in the form of a Discovery Grant from NSERC (Canada) and a CPU allocation from Compute Canada's WestGrid. The authors also acknowledge assistance from Rob Scharein with KnotPlot and that some figures were produced using Rob Scharein's KnotPlot [46].

References

[1] E. J. Janse van Rensburg. *The Statistical Mechanics of Interacting Walks, Polygons, Animals, and Vesicles*. 2nd ed. Oxford University Press, 2015. DOI: 10.1093/acprof:oso/9780199666577.001.0001.

[2] C. Vanderzande. *Lattice Models of Polymers*. Cambridge University Press (CUP), 1998. DOI: 10.1017/cbo9780511563935.

[3] A. J. Guttmann, ed. *Polygons, Polyominoes and Polycubes*. Vol. 775. Lecture Notes in Physics. Springer-Verlag Berlin, 2009. DOI: 10.1007/978-1-4020-9927-4.

[4] S. G. Whittington. "Statistical Mechanics of Polymer Solutions and Polymer Adsorption". In: vol. 51. Advances in Chemical Physics. Wiley-Blackwell, 1982, pp. 1–48. DOI: 10.1002/9780470142752.ch1.

[5] A. J. Guttmann and S. G. Whittington. "Two-dimensional lattice embeddings of connected graphs of cyclomatic index two". In: *J. Phys. A: Math. Gen.* **11**.4 (1978), p. 721. DOI: 10.1088/0305-4470/11/4/013.

[6] S. G. Whittington and J. P. Valleau. "Estimation of the Number of Self-Avoiding Lattice Polygons". In: *J. Chem. Phys.* **50**.11 (1969), pp. 4686–4690. DOI: 10.1063/1.1670956.

[7] D. W. Sumners and S. G. Whittington. "Knots in self-avoiding walks". In: *J. Phys. A: Math. Gen.* **21**.7 (1988), p. 1689. DOI: 10.1088/0305-4470/21/7/030.

[8] M. Delbrück and F. B. Fuller. "Knotting problems in biology". In: *Mathematical Problems in the Biological Sciences*. Ed. by R. E. Bellman. Vol. 14. Proceedings of Symposia in Applied Mathematics. American Mathematical Society, Providence, R.I., 1962, pp. 55–68. DOI: 10.1090/psapm/014.

[9] H. L. Frisch and E. Wasserman. "Chemical Topology". In: *J. Amer. Chem. Soc.* **83**.18 (1961), pp. 3789–3795. DOI: 10.1021/ja01479a015.

[10] N. C. H. Lim and S. E. Jackson. "Molecular knots in biology and chemistry". In: *J. Phys.: Condensed Matter* **27**.35 (2015), p. 354101. DOI: 10.1088/0953-8984/27/35/354101.

[11] E. Orlandini. "Statics and dynamics of DNA knotting". In: *J. Phys. A: Math. Theor.* **51** (2018), p. 053001. DOI: 10.1088/1751-8121/aa9a4c.

[12] E. J. Janse van Rensburg and S. G. Whittington. "The knot probability in lattice polygons". In: *J. Phys. A: Math. Gen.* **23**.15 (1990), p. 3573. DOI: 10.1088/0305-4470/23/15/028.

[13] V. Katritch, W. K. Olson, A. Vologodskii, J. Dubochet, and A. Stasiak. "Tightness of random knotting". In: *Phys. Rev. E* **61**.5 (2000), pp. 5545–5549. DOI: 10.1103/PhysRevE.61.5545.

[14] M. K. Shimamura and T. Deguchi. "Characteristic length of random knotting for cylindrical self-avoiding polygons". In: *Phys. Letts. A* **274**.5 (2000), pp. 184 –191. DOI: https://doi.org/10.1016/S0375-9601(00)00545-4.

[15] E. Uehara and T. Deguchi. "Characteristic length of the knotting probability revisited". In: *J. Phys.: Condensed Matter* **27**.35 (2015), p. 354104. DOI: 10.1088/0953-8984/27/35/354104.

[16] E. Uehara and T. Deguchi. "Knotting probability of self-avoiding polygons under a topological constraint". In: *J. Chem. Phys.* **147**.9 (2017), p. 094901. DOI: 10.1063/1.4996645.

[17] M. Baiesi and E. Orlandini. "Universal properties of knotted polymer rings". In: *Phys. Rev. E* **86** (2012), p. 031805. DOI: 10.1103/PhysRevE.86.031805.

[18] M. A. Cheston, K. McGregor, C. E. Soteros, and M. L. Szafron. "New evidence on the asymptotics of knotted lattice polygons via local strand-passage models". In: *J. Stat. Mech. Theor. Exp.* **2014**.2 (2014), P02014. DOI: 10.1088/1742-5468/2014/02/P02014.

[19] E. J. Janse van Rensburg. "Thoughts on lattice knot statistics". In: *J. Math. Chem.* **45**.1 (2008), p. 7. DOI: 10.1007/s10910-008-9364-9.

[20] E. J. Janse van Rensburg and A. Rechnitzer. "On the universality of knot probability ratios". In: *J. Phys. A: Math. Theor.* **44**.16 (2011), p. 162002. DOI: 10.1088/1751-8113/44/16/162002.

[21] E. Orlandini, M. C. Tesi, E. J. Janse van Rensburg, and S. G. Whittington. "Asymptotics of knotted lattice polygons". In: *J. Phys. A: Math. Gen.* **31**.28 (1998), p. 5953. DOI: 10.1088/0305-4470/31/28/010.

[22] A. Yao, H. Matsuda, H. Tsukahara, M. K. Shimamura, and T. Deguchi. "On the dominance of trivial knots among SAPs on a cubic lattice". In: *J. Phys. A: Math. Gen.* **34**.37 (2001), p. 7563. DOI: 10.1088/0305-4470/34/37/310.

[23] S. G. Whittington. "Knot probabilities for equilateral random polygons in $\mathbb{R}^3$". Presentation at *33rd Summer Conference on Topology and its Applications*, Western Kentucky University. 2018.

[24] E. Orlandini and S. G. Whittington. "Statistical topology of closed curves: Some applications in polymer physics". In: *Rev. Modern Phys.* **79** (2007), pp. 611–642. DOI: 10.1103/revmodphys.79.611.

[25] C. Micheletti, D. Marenduzzo, and E. Orlandini. "Polymers with spatial or topological constraints: Theoretical and computational results". In: *Physics Reports* **504**.1 (2011), pp. 1–73. DOI: 10.1016/j.physrep.2011.03.003.

[26] S. G. Whittington. "Self-avoiding walks with geometrical constraints". In: *J. Stat. Phys.* **30**.2 (1983), pp. 449–456. DOI: 10.1007/BF01012318.

[27] J. M. Hammersley and S. G. Whittington. "Self-avoiding walks in wedges". In: *J. Phys. A: Math. Gen.* **18**.1 (1985), p. 101. DOI: 10.1088/0305-4470/18/1/022.

[28] C. E. Soteros and S. G. Whittington. "Polygons and stars in a slit geometry". In: *J. Phys. A: Math. Gen.* **21**.17 (1988), p. L857. DOI: 10.1088/0305-4470/21/17/007.

[29] S. G. Whittington and C. E. Soteros. "Polymers in Slabs, Slits, and Pores". In: *Israel J. Chem.* **31**.2 (1991), pp. 127–133. DOI: 10.1002/ijch.199100014.

[30] C. E. Soteros, D. W. Sumners, and S. G. Whittington. "Linking of random p-spheres in $\mathbb{Z}^d$". In: *J. Knot Theory Ramifications* **08**.01 (1999), pp. 49–70. DOI: 10.1142/S0218216599000067.

[31] M. C. Tesi, E. J. Janse van Rensburg, E. Orlandini, and S. G. Whittington. "Knot probability for lattice polygons in confined geometries". In: *J. Phys. A: Math. Gen.* **27**.2 (1994), p. 347. DOI: 10.1088/0305-4470/27/2/019.

[32] M. C. Tesi, E. J. Janse van Rensburg, E. Orlandini, and S. G. Whittington. "Topological Entanglement Complexity of Polymer Chains in Confined Geometries". In: *Topology and Geometry in Polymer Science*. Ed. by S. G. Whittington, D. W. Sumners, and T. Lodge. Springer New York, 1998, pp. 135–157. DOI: 10.1007/978-1-4612-1712-1˙11.

[33] C. E. Soteros. "Knots in graphs in subsets of $\mathbb{Z}^3$". In: *Topology and Geometry in Polymer Science*. Ed. by S. G. Whittington, D. W. Sumners, and T. Lodge. Springer New York, 1998, pp. 101–133. DOI: 10.1007/978-1-4612-1712-1˙10.

[34] N. R. Beaton, J. W. Eng, K. Ishihara, K. Shimokawa, and C. E. Soteros. "Characterising knotting properties of polymers in nanochannels". In: *Soft Matter* **14**.28 (2018), pp. 5775–5785. DOI: 10.1039/C8SM00734A.

[35] M. Atapour, N. R. Beaton, J. W. Eng, K. Ishihara, K. Shimokawa, C. E. Soteros, and M. Vazquez. "Unknotting operations on 4-plat diagrams and the entanglement statistics of polygons in a lattice tube". In preparation.

[36] N. R. Beaton, J. W. Eng, and C. E. Soteros. "Polygons in restricted geometries subjected to infinite forces". In: *J. Phys. A: Math. Theor.* **49**.42 (2016), p. 424002. DOI: 10.1088/1751-8113/49/42/424002.

[37] M. Atapour, C. E. Soteros, and S. G. Whittington. "Stretched polygons in a lattice tube". In: *J. Phys. A: Math. Theor.* **42**.32 (2009), p. 322002. DOI: 10.1088/1751-8113/42/32/322002.

[38] C. E. Soteros and S. G. Whittington. "Lattice models of branched polymers: effects of geometrical constraints". In: *J. Phys. A: Math. Gen.* **22**.24 (1989), pp. 5259–5270. DOI: 10.1088/0305-4470/22/24/014.

[39] A. Kloczkowski and R. L. Jernigan. "Transfer matrix method for enumeration and generation of compact self-avoiding walks. II. Cubic lattice". In: *J. Chem. Phys.* **109**.12 (1998), pp. 5147–5159. DOI: 10.1063/1.477129.

[40] J. W. Eng. "Self-Avoiding Polygons in (L, M)-Tubes". Master's thesis. University of Saskatchewan, 2014.

[41] M. Atapour. "Topological Entanglement Complexity of Systems of Polygons and Walks in Tubes". PhD thesis. University of Saskatchewan, 2008.

[42] C. E. Soteros, D. W. Sumners, and S. G. Whittington. "Entanglement complexity of graphs in $\mathbb{Z}^3$". In: *Math. Proc. Cambridge Phil. Soc.* **111**.01 (1992), p. 75. DOI: 10.1017/s0305004100075174.

[43] S. E. Alm and S. Janson. "Random self-avoiding walks on one-dimensional lattices". In: *Comm. Stats. Stochastic Models* **6**.2 (1990), pp. 169–212. DOI: 10.1080/15326349908807144.

[44] R. Scharein, K. Ishihara, J. Arsuaga, Y. Diao, K. Shimokawa, and M. Vazquez. "Bounds for the minimum step number of knots in the simple cubic lattice". In: *J. Phys. A: Math. Theor.* **42**.47 (2009), p. 475006. DOI: 10.1088/1751-8113/42/47/475006.

[45] E. J. Janse van Rensburg. "Monte Carlo methods for the self-avoiding walk". In: *J. Phys. A: Math. Theor.* **42**.32 (2009), p. 323001. DOI: 10.1088/1751-8113/42/32/323001.

[46] R. Scharein. "The KnotPlot Site". URL: https://www.knotplot.com/.

[47] R. Stolz, M. Yoshida, R. Brasher, M. Flanner, K. Ishihara, D. J. Sherratt, K. Shimokawa, and M. Vazquez. "Pathways of DNA unlinking: A story of stepwise simplification". In: *Sci. Rep.* **7** (2017), p. 12420. DOI: 10.1038/s41598-017-12172-2.

[48] T. Williams, C. Kelley, and many others. "Gnuplot". `http://www.gnuplot.info/`.

[49] K. Ishihara, M. Pouokam, A. Suzuki, R. Scharein, M. Vazquez, J. Arsuaga, and K. Shimokawa. "Bounds for minimum step number of knots confined to tubes in the simple cubic lattice". In: *J. Phys. A: Math. Theor.* **50**.21 (2017), p. 215601. DOI: 10.1088/1751-8121/aa6a4f.